Tidal Turbine Benchmarking Exercise: Geometry Specification and Environmental Characterisation

S.W. Tucker Harvey, X. Chen, D. Rowe, K. Bhavsar, T. Allsop, J. Gilbert, T. Stallard, C.R. Vogel and R.H.J. Willden

Abstract—**Uncertainty in tidal turbine loading contributes significantly to conservatism in turbine design. This uncertainty originates not only from a lack of knowledge of the flow field at a particular site, but also from lack of understanding of the fundamental physics which govern the loading and performance of tidal turbines in unsteady and turbulent flow regimes. In order to reduce this conservatism and the costs associated, the mathematical and engineering models used in turbine design must be improved. To facilitate the development of these models requires scale experimental data for validation. However, few well-documented experimental data sets are available for tidal turbines, especially at scales large enough to achieve Reynolds number independence and comparability to full scale devices.**

This paper reports on the initial phases of a tidal turbine benchmarking project that will conduct a large laboratory scale experimental campaign on a highly instrumented 1.6m diameter tidal rotor. The turbine will be tested in well-defined flow conditions, including unsteadiness created by free surface waves, as well as freestream turbulence, with instrumentation to determine edgewise and flapwise loading distributions along the blades as they rotate through the unsteady flows. As towing tanks by their nature have low levels of freestream turbulence, a carriage-mounted turbulence grid will be utilised to generate sufficient freestream turbulence in a well-defined manner.

In this paper the turbine geometry and test conditions are specified, as well as providing details of the rotor's hydrodynamic design process. Additionally, the results of a flow characterisation of the carriage-mounted turbulence grid via Acoustic Doppler Velocimetry are presented. The turbulence grid produced a mean turbulence intensity of 3.5% across the region in which the turbine will be tested, and a very uniform flow profile of 0.913 times the upstream velocity.

Index Terms—**Tidal Turbines, Benchmarking, Unsteady Turbine Fluid Mechanics**

I. Introduction

Tidal stream energy is an underutilised renewable resource that could provide a significant contribution to future renewable energy production. However, the sector faces sizeable technical challenges, such as the hostile hydrodynamic environment in which devices operate. The presence of large-scale turbulent vortices and wave generated unsteadiness in tidal stream sites leads to uncertainty in tidal turbine loading and drives conservatism in design. In order to reduce this conservatism, the mathematical and engineering models used in turbine design must be improved, requiring large-scale experiment data for model validation.

Numerous laboratory scale experiments on model tidal turbines have been performed, with notable examples including the work of Bahaj [1], Gaurier [2] and Payne [3]. A number of different flow conditions and operational regimes have been investigated including regular waves [4], yawed flow [5] and turbulence [6]. However, few well-documented data sets are available for model validation, especially at scales large enough to provide Reynolds number independence and thus closer applicability to full scale devices.

The tidal turbine benchmarking project, funded by the UK's EPSRC and the Supergen Offshore Renewable Energy Hub, will conduct a large laboratory scale experiment on a highly instrumented $1.6\,\mathrm{m}$ diameter tidal rotor. The turbine will be instrumented for the measurement of spanwise distributions of flapwise and edgwise bending moments and will be tested in well-defined flow conditions, including wave generated unsteadiness and freestream turbulence. The turbine will be pushing through a long towing tank to achieve the required incident current and wave conditions. In order to achieve higher levels of freestream turbulence a $2.4\,\mathrm{m}$ by $2.4\,\mathrm{m}$ turbulence grid has been designed, manufactured and tested in the tow tank, and will be towed upstream of the turbine in the later turbine experiments. The experimental testing will be followed by two rounds of blind benchmarking in which engineers from academia and industry will be invited to predict the loading experienced by the turbine under prescribed turbulence and wave conditions. The benchmarking rounds and staged release of experimental data will enable engineers to understand the limitations of their models and provide data to enable modelling improvements.

In this paper the test conditions, turbine geometry and further parameters for the benchmarking experiment are specified. Details of the hydrodynamic design process are also provided, including outlines of the foil selection, trailing edge treatment and Reynolds-Averaged Navier Stokes (RANS) - Blade Element design simulations. Additionally, further insight into the designed blade hydrodynamics is gained by high fidelity blade resolved simulations. Finally, the results

Paper ID 2276 submitted to Tidal device development and testing.

Authors S.W. Tucker Harvey, D. Rowe, X. Chen, C.R Vogel and R.H.J. Willden are affiliated with the Department of Engineering Science, University of Oxford, Oxford OX1 3PJ, United Kingdom (e-mail: sam.harvey@eng.ox.ac.uk)

Authors K. Bhavsar, T. Allsop and J. Gilbert are affiliated with the Faculty of Science and Engineering, University of Hull.

Author T. Stallard is affiliated with the Department of Mechanical, Aerospace and Civil Engineering, University of Manchester.

of an initial flow characterisation of the turbulence grid using an Acoustic Doppler Velocimeter (ADV) are presented.

II. Test Facility and Test Conditions

For a benchmarking exercise to be effective, the flow conditions must be closely controllable, while the level of global blockage should be low. Towing tank facilities are hence well suited due to their typically large section size and well-defined flow velocity. The QinetiQ towing tank facility based in Haslar, Portsmouth UK, has been selected for the benchmarking exercise and has dimensions of $270\,\mathrm{m}$ (L) $\times$ $12.2\,\mathrm{m}$ (W) $\times$ $5.4\,\mathrm{m}$ (D). The QinetiQ facility is also capable of producing waves with amplitudes up to $0.37\,\mathrm{m}$ and wave frequencies between $0.2\,\mathrm{Hz}$ and $1\,\mathrm{Hz}$. The level of freestream turbulence is generally very low in towing tank facilities, and hence, to provide a higher level of turbulence, a carriage-mounted turbulence grid will be implemented for the benchmarking experiment. The key parameters of the test, as well as the benchmarking turbine are tabulated in table II. An illustration of the experimental setup for the benchmarking exercise is shown in Fig. 1. The turbulence grid is mounted to the front of the QinetiQ towing tank carriage allowing the turbulence to develop before reaching the turbine plane close to the carriage rear section.

TABLE I
Benchmarking experiment parameters

Quantity	Symbol	Unit	Value
Turbine diameter	D	m	1.6
Nacelle diameter	D_n	m	0.2
Number of blades	N_b	–	3
Hub depth	d_h	m	1.33
Turbulence Grid Width	W_g	m	2.4
Distance from Grid to Turbine plane	L_x	m	5.0
Flow velocity	U_∞	ms^{-1}	1.0
Blockage Ratio	B_r	%	3.05

III. Turbine Hydrodynamic Design

A. Hydrofoil performance

Following the specification of the operational environment, the next stage in the hydrodynamic design process of a tidal turbine is the selection of the blade profile. The NACA 63-415 profile was selected as the blade profile for the benchmarking rotor. This profile, and its family variation 63-815, have been successfully used in a number of different tidal turbine designs, such as the model test turbine used by Alstom company (now part of GE power) [7], the MCT experimental tidal turbine built by the research group from the University of Southampton [1], and the X-MED experimental tidal turbine by the research group from the University of Manchester [3].

For simplicity of design and ease of specification in the later blind prediction phases we choose to use a single blade profile along the entire blade span. Due to both safety and manufacturing considerations, the

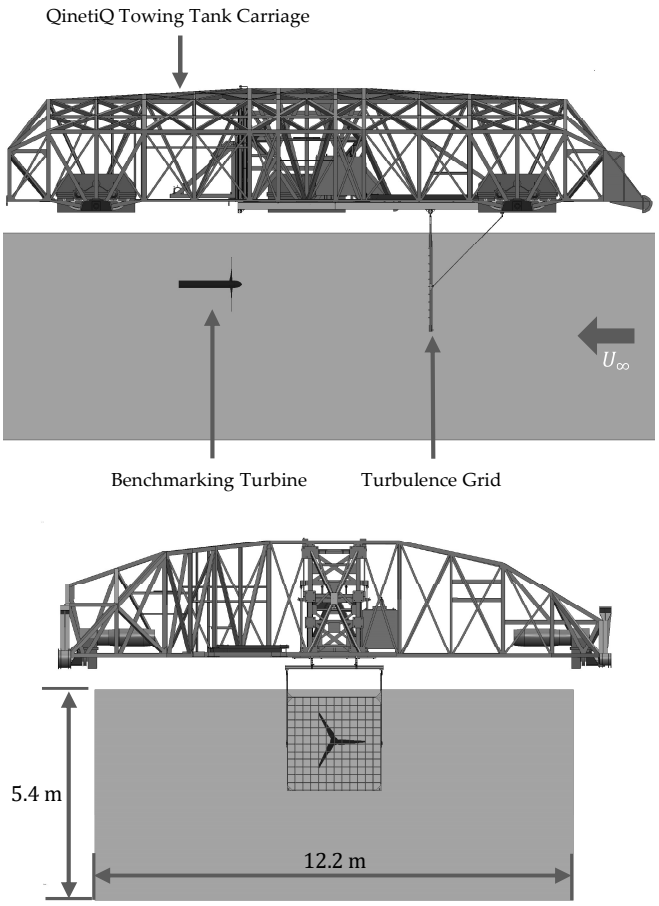

Fig. 1. Illustration of setup for the benchmarking experiment.

trailing edge of the profile must be thickened from the zero thickness in the original profile. This must be achieved with care so as not to significantly alter the two-dimensional blade foil characteristics. One approach to implementing this thickening is to truncate the profile ahead of the trailing edge, however this can result in significant changes to the performance of the profile. Trailing portion thickening functions offer an alternative to blade truncation and when applied carefully to both sides of the foil do not alter camber and minimally alter foil performance. We choose to use a thickening function which we have successfully employed in Oxford's previous successful $1.2\,\mathrm{m}$ tidal turbine experiments [8]. The thickening function implemented for the benchmarking blade profile is defined by the equation,

$$y_t = \begin{cases} y_0, & 0 \le x \le x_T, \\ y_0 \pm 0.5\delta \left(\frac{x-x_T}{c-x_T}\right)^n & x_T \le x \le c. \end{cases} \quad (1)$$

where x and y_0 denote the coordinates of the original sharp profile, y_t is the y coordinate of the thickened profile, x_T denotes the x coordinate at which the thickened profile separates from the original profile, and the thickening by $+/-$ are used for suction and pressure surfaces respectively. The thickness at the trailing edge is represented by δ, chosen to be $0.00625c$ for the benchmarking blade profile, where c is the chord length. The parameter n defines the shape of

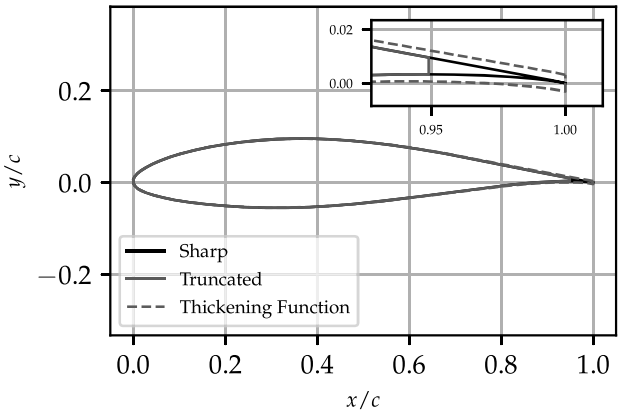

Fig. 2. Illustration of airfoil trailing edge treatments. Profile coordinates x and y are shown non-dimensionalised with the chord length c. Both thickening methods provide a trailing edge thickess of $0.00625c$.

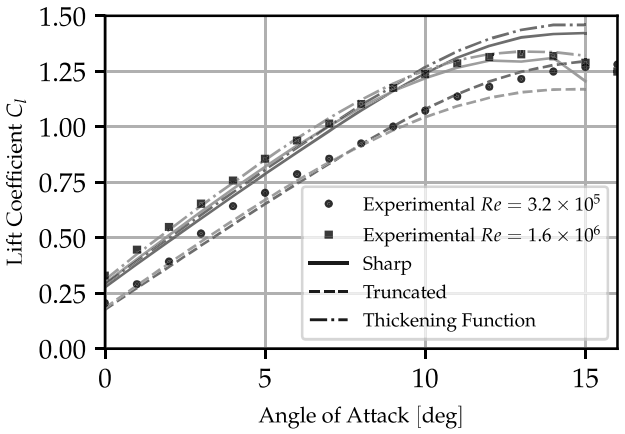

Fig. 3. Lift coefficient of NACA 63-415. Orange lines: tip turbulence intensity (∼1.3%), blue lines: hub turbulence intensity (∼8%).

the thickened section of the profile and was set to 2.0. A comparison between the trailing edge thickened, trailing edge truncated and the original sharp profile is illustrated in Fig. 2.

To investigate the influence of the different thickening methods on the profile hydrodynamic performance, two-dimensional Computational Fluid Dynamics (CFD) simulations using the RANS approach with SST $\mathrm{k}-\omega$ turbulence closure were performed comparing profiles thickened with the two methods to the original sharp profile. The simulated lift and drag coefficient, as well as the lift-to-drag ratio are presented in Fig. 3, 4 and 5.

We make comparison to experimental data at two Reynolds numbers 3.2×10^5 [9] and 1.6×10^6 [10], with the lower being representative of large laboratory experiments and the higher representative of field conditions. The lower Re experimental data exhibits lower lift, higher drag, and consequently lower lift-to-drag across the full range of angles of attack. In our simulations of hydrofoil performance we consider two turbulence intensities, 1.3% and 8%, as the turbulence intensity in the frame of the blade increases from blade tip to root.

The truncated trailing edge treatment results in a significant reduction in lift as well as a more modest reduction in drag coefficient, which collectively lead to a reduction in the lift-to-drag ratio between the sharp and truncated profiles. Meanwhile, the thickening function successfully maintains a close performance in both lift and drag compared to the sharp trailing edge profile. Using the thickening function is therefore advantageous as it provides flexibility in modelling approaches that may be employed in the later benchmarking phases; CFD investigation may choose to use sharp trailing edges for efficiency, whilst Blade Element Momentum (BEM) or actuator line type simulations can utilise either sharp or thickened foil performance data with little modelling difference.

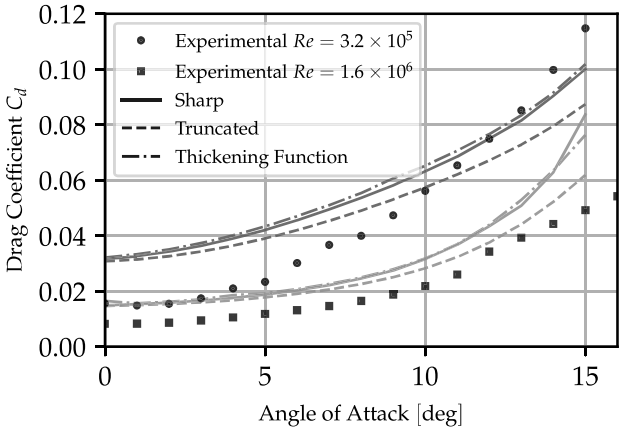

Fig. 4. Drag coefficient of NACA 63-415. Orange lines: tip turbulence intensity (∼1.3%), blue lines: hub turbulence intensity (∼8%).

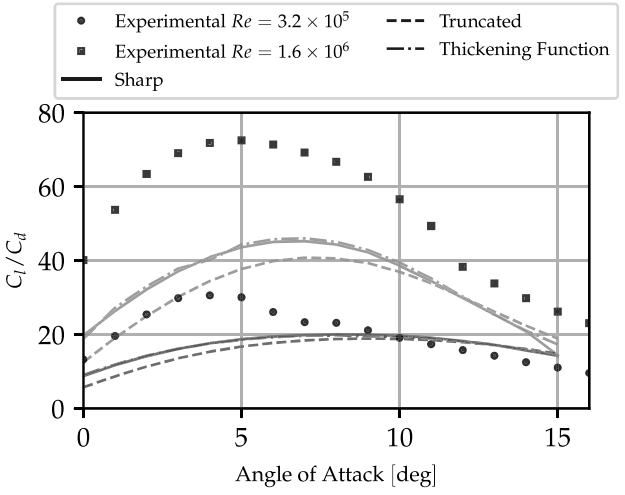

Fig. 5. Lift-to-drag ratio of NACA 63-415. Orange lines: tip turbulence intensity (∼1.3%), blue lines: hub turbulence intensity (∼8%).

B. Blade design

The rotor blades were designed using a blade element actuator disk method, embedded in a RANS-BE implemented in OpenFOAM. More details of the method can be found in [8].

As stated in the test conditions, the turbine will be operating at a blockage ratio of 3.05% and was originally designed for an upstream turbulence intensity of 8%. The blockage ratio in the design simulation follows the same blockage ratio, with a cylindrical channel as shown in Fig. 6. It is also found that the blade sectional turbulence intensity has a large influence on the hydrodynamic performance, especially of the drag coefficient, as the orange and blue curves in Fig. 4 and 5 illustrate. Hence, the design simulation also takes the sectional turbulence intensity into account, which offers an improvement in fidelity of prediction over more standard BEM and RANS-BE design approaches.

A design process was followed whereby the tip-speed ratio is set to a desired value, $TSR = 6$, and the blade twist and chord iteratively altered to achieve a near optimal local loading distribution and the design angle-of-attack, 6°, along the entire length of the blade (the design angle-of-attack is taken as the peak of the lift-to-drag sectional data, see Fig. 5). The resulting design parameters (chord length and twist angle) for the benchmarking rotor are presented in Fig. 7. A rendered image of the blade geometry and simplified nacelle are shown in Fig. 8.

Once the blade design was complete, higher fidelity blade resolved RANS simulations in a rotating frame of reference allowed the RANS-BE design simulations to be verified and provided some further insight into the blade hydrodynamics. A single blade was simulated in a 120° wedge, exploiting the rotational symmetry of the benchmarking rotor as illustrated in Fig. 8. The structures of the tip and root vortices are visualised in Fig. 9a by isosurfaces of the λ_2 vortex criterion. The isosurfaces are coloured by the non-dimensional streamwise velocity. Blade surface streamlines provide additional insight into the root and tip effects and are illustrated in Fig. 9b and Fig. 9c on the pressure and suction surfaces respectively.

Further details on the computed performance of the rotor will be released following the blind prediction phases of this project.

IV. Instrumentation and Measurement Techniques

A. Benchmark Turbine Instrumentation

Fig. 10 provides an overview of the construction of the benchmarking experimental turbine. All three blades of the benchmarking turbine are instrumented for spanwise distributions of flapwise and edgewise bending moments. Two of the blades are instrumented with strain gauges, while the remaining blade provides the measurements with fibre Bragg sensors (FBG). The interrogator, light source and optical switch required for the FBG measurements are mounted within the turbine nosecone, while the strain gauge amplifiers are

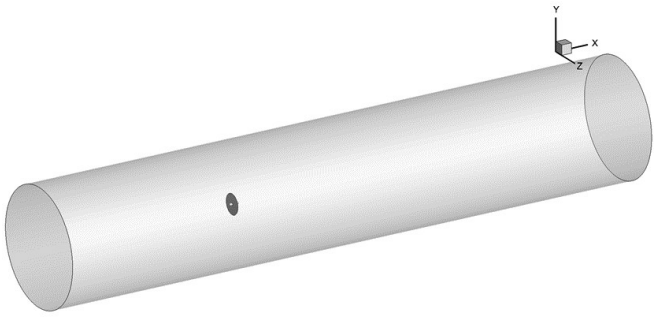

Fig. 6. Cylindrical domain for RANS-BE design simulations. Rotor disk shown darker towards the centre of the domain. Inflow is at the left hand end.

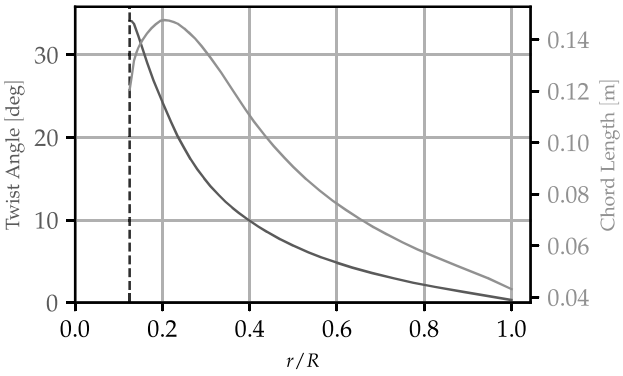

Fig. 7. Blade design parameters. The nacelle radial position is illustrated by the dashed line.

contained within an additional section mounted behind the turbine hub. In addition to the in-blade instrumentation, measurements of root bending moments in the flapwise and edgewise directions are provided by strain gauges integrated into the hub component.

To determine the rotor's coefficients of performance and thrust requires accurate measurement of the torque, thrust and angular velocity. Torque and thrust measurements are provided by a torque and thrust transducer positioned behind the strain gauge amplifier section and mounted ahead of the upstream bearing, so as to minimise loses, to the end of the drive shaft. A rotary encoder gives the angular position and

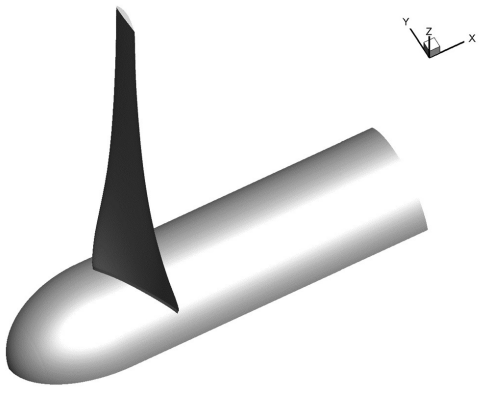

Fig. 8. Illustration of geometry used in blade resolved simulations.

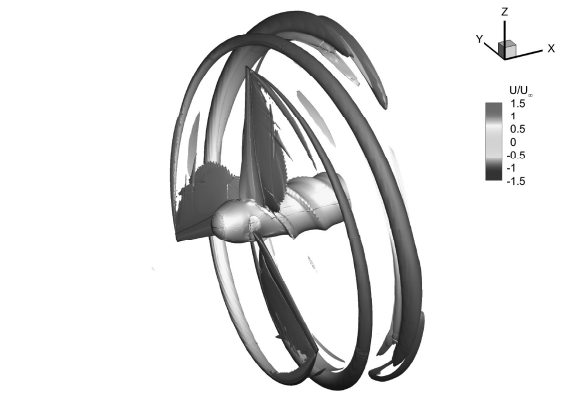

(a) Isosurfaces of λ_2 vortex criterion.

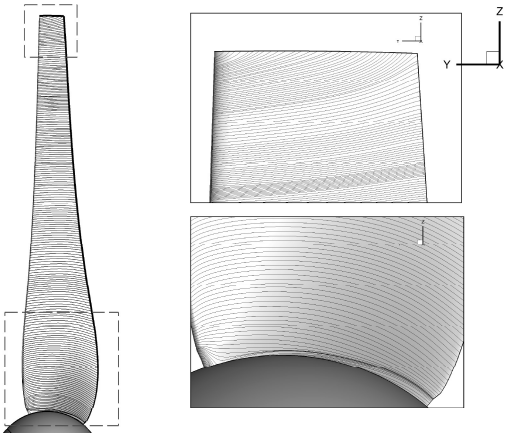

(b) Blade surface streamlines: pressure side.

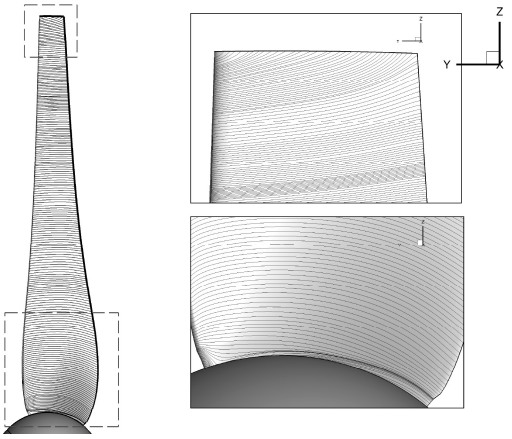

(c) Blade surface streamlines: suction side.

Fig. 9. Flow visualisations of blade-resolved CFD simulations of the benchmarking rotor.

hence angular velocity of the rotor.

For the blades to be instrumented for the spanwise distributions of flapwise and edgewise bending moments, the blades were constructed from two parts, a main body with a slotted section along the pressure surface and an insert part. By adhering the insert into the main body of the blade, the blade geometry is completed whilst leaving a cavity within to hold the instrumentation. Fig. 11 illustrates the construction of the instrumented blades. The slot is designed around the blade's neutral axis and is made as large as possible as so as to improve the sensitivity of measurements.

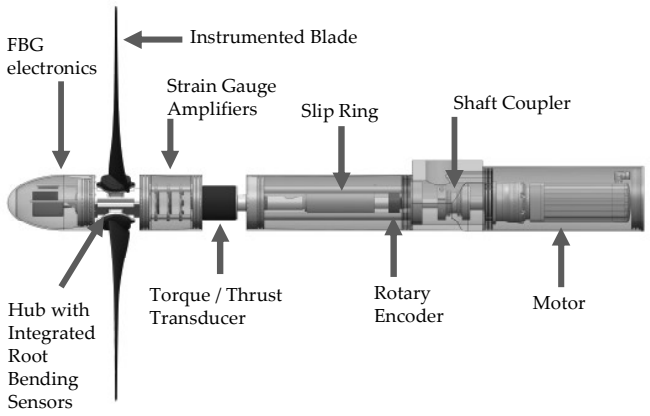

Fig. 10. Illustration of benchmarking turbine construction.

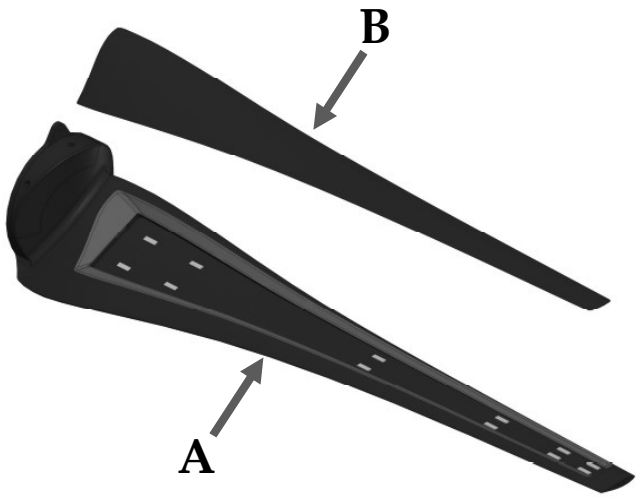

Fig. 11. Illustration of instrumented blade construction. A denotes the main body of the blade, whilst B is the insert component. Example strain gauge locations are also illustrated as lighter coloured rectangular areas.

A total of six measurement locations will be used in the flapwise direction and five in the edgewise direction on each blade. These span from $r/R = 0.225$ to $r/R = 0.948$.

B. Turbulence Grid Design

A carriage-mounted turbulence grid was developed with the objective of elevating the low levels of freestream turbulence in the QinetiQ towing tank facility. The grid was located at a distance of $L_x = 5.0\,\mathrm{m}$ upstream of the intended turbine plane and was constructed of aluminium bars of rectangular section mounted to an outer frame. This construction allows for adjustable porosity, and hence a variable level of turbulence produced, by varying the number of bars fixed to the outer frame. The grid geometry was constrained by the force limits of the QinetiQ towing tank carriage, resulting in the selection of a bar width of $15\,\mathrm{mm}$, yielding porosities θ (ratio of open area to total grid frontal area) of 0.95, 0.91 and 0.84 for the three

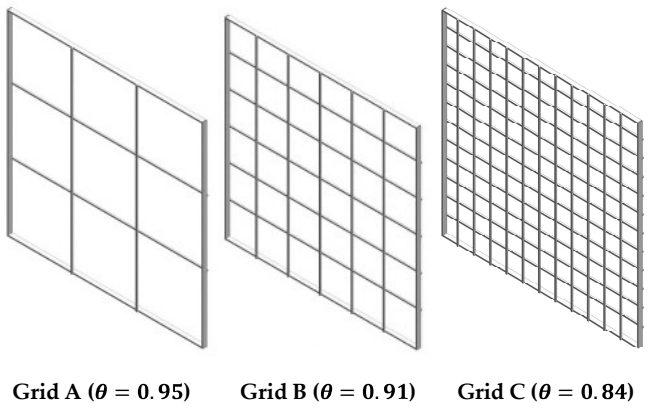

Fig. 12. Illustration of turbulence grid configurations.

Fig. 13. Image of turbulence grid configuration C in operation in the QinetiQ towing tank.

turbulence grid configurations chosen for the experiments. Fig. 12 illustrates the selected grid geometries. An image showing the turbulence grid configuration C in operation in the towing tank is shown in Fig 13.

V. Flow Characterisation of Turbulence Grid Wake

A. Methodology

Before experiments are performed with the benchmarking turbine positioned downstream of the turbulence grid, the flow behind the grid at the intended turbine plane must be characterised. Acoustic Doppler Velocimeter (ADV) measurements were obtained with a Nortek Vectrino ADV positioned close to the turbine plane, providing a measurement of the inflow that will be experienced by the benchmarking turbine.

To provide sufficient back-scatter for the successful operation of the ADV in the QinetiQ towing tank facility, the tank was seeded prior to each pair of tows with Spherical 110P8 Inorganic Microspheres, provided by Potters Industries. A $410\,\mathrm{L}$ volume of seeded water with a particle concentration of $0.3\,\mathrm{gL}^{-1}$ was introduced into the tank at each measurement position with a carriage velocity of $0.5\,\mathrm{ms}^{-1}$ over a distance of $150\,\mathrm{m}$.

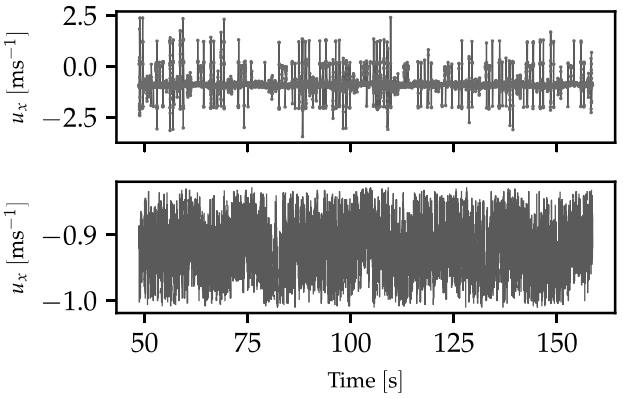

Fig. 14. Example of spike identification and removal in ADV velocity signal. Upper plot: The blue line is the raw streamwise velocity signal, while the red points illustrate the locations of the identified spikes. Lower plot: the blue line is the filtered velocity signal.

Over the course of the testing campaign over 10 tonnes of seeding fluid was injected into the tank.

In the testing procedure, a tow was performed to first seed the flow, with the seeding fluid injected at either two or three locations in the turbulence grid. Following this the tank was allowed to settle for 15 minutes, after which the first tow at a speed of $1\,\mathrm{ms}^{-1}$ was performed to record velocities at the seeded locations with two or three ADVs simultaneously. The tank was then allowed to settle again for 15 mins following which a repeat tow was performed.

Measurements were taken across a stencil one upper quadrant of the grid. This stencil consisted of a vertical profile, a horizontal profile and a diagonal profile, as well as some additional positions in other quadrants to demonstrate horizontal and vertical symmetry of the generated profile. In total of 19 measurement locations were sampled.

Velocity signals obtained with ADVs are often effected by Doppler noise and aliasing, resulting in erroneous spikes. The removal of anomalous results in the velocity signals was performed with the velocity correlation filter described by Cea et al. [11]. Fig. 14 provides an example of the identification of spikes in the streamwise velocity component and subsequent filtering.

B. Results

The profile of the mean streamwise velocity measured along the vertical centre-line of the turbulence grid is illustrated in figure 15. The turbine nacelle axis will be located exactly at the centre of the upstream turbulence grid and hence we seek to measure the profile and turbulence from the centre of the nacelle, $z = 0\,\mathrm{m}$, to the edge of the rotor, $z = 0.8\,\mathrm{m}$, and all of the way to the edge of the grid, $z = 1.2\,\mathrm{m}$. The mean streamwise velocity can be seen to reach a minimum value of $0.913\,U_\infty$ at the centre of the grid and increases towards the grid edge, although it does not recover fully to the free-stream velocity indicating that the grid wake is significantly wider than the grid at this distance downstream of it. Averaging over the region

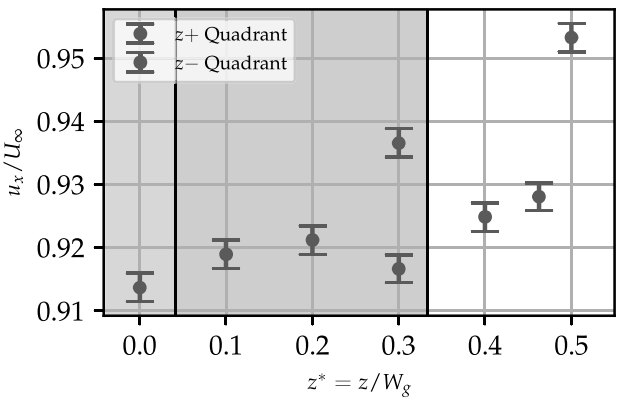

Fig. 15. Vertical profile of streamwise velocity measured close to the location of the turbine plane. The blue and red points were obtained in the upper and lower half of the grid, above and below the turbine nacelle axis respectively. The green shading highlights the extent of the blade, while the yellow shading shows the radial extent of the turbine nacelle. The error indicated by the error-bars is calculated from the average range of two repeats.

that is intended to be occupied by the benchmarking turbine yields an average flow velocity of $0.917\,U_\infty$. The profile is observed to remain highly uniform across this region with only an $\pm 0.5\%$ variation around this mean wake velocity. Similar uniformity of profile was observed in both the horizontal and diagonal transects.

Defining the turbulence intensity as

$$I_i = \frac{u'_{i\,\mathrm{rms}}}{\sqrt{\bar{u}_x^2 + \bar{u}_y^2 + \bar{u}_z^2}}, \tag{2}$$

where I_i denotes the turbulence intensity in the i^{th} direction, $u'_{i\,rms}$ is the root mean square of the fluctuating velocity component and $\bar{u}_i$ denotes the mean velocity in each direction. The turbulence intensity in the streamwise direction was found to be between 2.9% and 4.3% with a mean value of 3.5%.

VI. Conclusions

The tidal turbine benchmarking exercise aims to assist in the improvement of the mathematical and engineering models used in turbine design by providing a well-documented large-scale data set to be used in model validation. In this paper the geometry of the benchmarking rotor has been specified, alongside the test facility and inflow turbulence conditions. The turbine RANS-BE hydrodynamic design process has been described, through which a design angle-of-attack and spanwise loading are targeted along the blade span. Particular attention has been paid to the method of trailing edge thickening so as not to alter the foil's hydrodynamic characteristics.

In order to generate sufficient levels of freestream turbulence in the towing tank, we have designed and implemented a carriage-mounted turbulence grid. Flow characterisation results obtained via Acoustic Doppler Velocimetry have shown the maximum velocity deficit behind the turbulence grid developed for the benchmarking experiment to be $0.913\,U_\infty$ and the flow remains highly uniform across the intended rotor location. The turbulence intensity has been found to be between 2.9% and 4.3% with a mean value of 3.5% in the region that will be occupied by the benchmarking turbine.

Acknowledgements

This benchmarking exercise is being funded by the Supergen ORE Hub, grant number EP/S000747/1, and by RHJW's EPSRC Advanced Fellowship EP/R007322/1. We would like to thank Catherine Wilson at the University of Cardiff for loan of ADV equipment. The authors are also grateful for the assistance of QinetiQ staff during the testing campaign.

References

[1] A. Bahaj, W. Batten, and G. McCann, "Experimental verifications of numerical predictions for the hydrodynamic performance of horizontal axis marine current turbines," *Renewable Energy*, vol. 32, no. 15, pp. 2479–2490, 2007. [Online]. Available: https://www.sciencedirect.com/science/article/pii/S0960148107002996

[2] B. Gaurier, G. Germain, J. Facq, C. Johnstone, A. Grant, A. Day, E. Nixon, F. Di Felice, and M. Costanzo, "Tidal energy "round robin" tests comparisons between towing tank and circulating tank results," *International Journal of Marine Energy*, vol. 12, pp. 87–109, 2015, special Issue on Marine Renewables Infrastructure Network. [Online]. Available: https://www.sciencedirect.com/science/article/pii/S2214166915000223

[3] G. S. Payne, T. Stallard, and R. Martinez, "Design and manufacture of a bed supported tidal turbine model for blade and shaft load measurement in turbulent flow and waves," *Renewable Energy*, vol. 107, pp. 312–326, 2017. [Online]. Available: https://www.sciencedirect.com/science/article/pii/S0960148117300782

[4] L. Luznik, K. A. Flack, E. E. Lust, and K. Taylor, "The effect of surface waves on the performance characteristics of a model tidal turbine," *Renewable Energy*, vol. 58, pp. 108–114, 2013. [Online]. Available: https://www.sciencedirect.com/science/article/pii/S0960148113001316

[5] P. W. Galloway, L. E. Myers, and A. S. Bahaj, "Quantifying wave and yaw effects on a scale tidal stream turbine," *Renewable Energy*, vol. 63, pp. 297–307, 2014. [Online]. Available: https://www.sciencedirect.com/science/article/pii/S0960148113004977

[6] B. Gaurier, M. Ikhennicheu, G. Germain, and P. Druault, "Experimental study of bathymetry generated turbulence on tidal turbine behaviour," *Renewable Energy*, vol. 156, pp. 1158–1170, 2020. [Online]. Available: https://www.sciencedirect.com/science/article/pii/S0960148120306340

[7] "Alstom's 1mw tidal stream turbine installed in scotland achieves 1 gwh power production," Alstom Press Release and News, 2014, [Online, accessed 2nd June 2021]. [Online]. Available: https://www.alstom.com/press-releases-news/2014/12

[8] J. McNaughton, B. Cao, S. Ettema, F. Z. de Arcos, C. Vogel, and R. Willden, "Experimental testing of the performance and interference effects of a cross-stream array of tidal turbines," in *Developments in Renewable Energies Offshore, Proceedings of the 4th International Conference on Renewable Energies Offshore*, 2020.

[9] H. Cerón-M, F. Catalano, and A. C. Filho, "Experimental study of the influence of vortex generators on airfoils for wind turbines," in *Conference: VI Congreso Internacional de Ingeniería Mecánica*, 05 2013.

[10] C. Bak, P. Fuglsang, J. Johansen, and I. Antoniou, "Wind tunnel tests of the naca 63-415 and a modified naca 63-415 airfoil," in *RISØ-R–1193*, 01 2000.

[11] L. Cea, J. Puertas, and L. Pena, "Velocity measurements on highly turbulent free surface flow using adv," *Experiments in fluids*, vol. 42, no. 3, pp. 333–348, 2007.